Thermodynamics of Statherin Adsorption onto Hydroxyapatite†

Rivka Goobes,‡,§ Gil Goobes,§,|| Charles T. Campbell,|| and Patrick S. Stayton*,‡

Departments of Bioengineering and Chemistry, University of Washington, Seattle, Washington 98195

Received November 12, 2005; Revised Manuscript Received February 20, 2006

ABSTRACT: Statherin is a salivary protein that inhibits the nucleation and growth of hydroxyapatite crystals in the supersaturated environment of the oral cavity. The thermodynamics of adsorption of statherin onto hydroxyapatite crystals have been characterized here by isothermal titration calorimetry and equilibrium adsorption isotherm analysis. At 25 °C, statherin adsorption is characterized by an exothermic enthalpy of ∼3 kcal/mol that diminishes to zero at ∼25% surface coverage. The initial heat of statherin adsorption increases with temperature, displaying a positive heat capacity change of 194 ± 7 cal K^{-1} mol^{-1} at 25 °C. The heat of adsorption during this initial phase is strongly dependent on the buffer species, and from the differential heats of buffer ionization, it can be calculated that approximately one proton is taken up by the crystal or protein upon adsorption. The free energy of adsorption is dominated at all coverages by a large positive entropy (≥23 cal K^{-1} mol^{-1}), which may be partially due to the loss of organized water that hydrates the protein and the mineral surface prior to adsorption. These results are interpreted using a two-site model for adsorption of statherin onto the hydroxyapatite crystals.

Organisms have evolved sophisticated mechanisms for controlling inorganic mineral growth to make high-performance composite materials such as bone and teeth, and to maintain their integrity. Statherin is a small salivary protein with a molecular mass of 5380 Da (*1*−*3*). It inhibits the nucleation and growth of hydroxyapatite in the oral cavity, which is supersaturated with respect to the ionic components of the mineral. The activity of statherin is critical since the supersaturated condition is needed to maintain tooth enamel, while mineral accretions must be kept from forming on the tooth surface or in the bulk saliva (*1*−*6*). The molecular mechanisms underlying statherin's interaction with hydroxyapatite have been actively studied to define how proteins function at the inorganic mineral interface. The direct hydroxyapatite binding contacts have been generally ascribed to the acidic side chains and two phosphoserines at the N-terminus of statherin (*5*, *7*). The adsorption of statherin onto hydroxyapatite has been previously characterized by Nancollas, and important relationships between adsorption coverage and functional hydroxyapatite growth properties were determined (*4*, *5*). Previous studies of the protein in aqueous solution indicated an essentially disordered structure (*8*, *9*). Structural and dynamics studies of statherin and statherin fragments adsorbed onto hydroxyapatite using high-resolution solid-state NMR have been carried out by our group more recently (*10*−*14*). The results directly demonstrated that the N-terminal domain is α-helical and that it contains residues that are close to the HAP[1] surface.

Thermodynamic characterization provides key mechanistic insight into the basis of protein function, but in the case of adsorption of a protein onto biologically relevant surfaces, there is relatively little experimental precedent. The free energy of adsorption is derived from equilibrium binding isotherm analysis after model assumptions are adopted (*15*). Measurement of the adsorption enthalpy allows separation of the adsorption free energy into its enthalpic and entropic contributions, thus providing new insight into the mechanistic aspects of adsorption. There have been two important areas where the mechanism of adsorption of proteins onto surfaces has been studied in this manner by calorimetry: the adsorption of proteins onto support materials used in liquid chromatography (*16*−*19*) and the adsorption of proteins onto polymeric surfaces in biomaterials and colloids (*20*−*27*). The adsorption of statherin as well as other salivary proteins onto HAP had been previously studied from equilibrium binding isotherm measurements (*4*, *5*, *28*−*30*). In an attempt to study the contribution of the enthalpy and entropy to the free energy of the adsorption of several proteins, their values were derived from the isotherms performed at different temperatures (*28*). Here we have jointly used isothermal titration calorimetry and equilibrium adsorption isotherm analysis to determine the thermodynamic parameters (equilibrium constant, free energy, enthalpy, entropy, and heat capacity) of adsorption of statherin onto hydroxyapatite crystals. The results lead to a two-site binding model that provides new

† This work was supported by funding from the National Institutes of Health (Grant DE12554) and the National Science Foundation (Grants 0502177 and 9807748).

* To whom correspondence should be addressed: Mail Stop 355061, Department of Bioengineering, University of Washington, Seattle, WA 98195-1721. Phone: (206) 685-8148. Fax: (206) 685-8256. E-mail: stayton@u.washington.edu.

‡ Department of Bioengineering.

§ Co-first authors.

|| Department of Chemistry.

[1] Abbreviations: CD, circular dichroism; DSC, differential scanning calorimetry; HAP, hydroxyapatite $Ca_{10}(OH)_2(PO_4)_6$; ITC, isothermal titration calorimetry; PB, phosphate buffer [100 mM NaCl, 40 mM KCl, 4.3 mM Na_2HPO_4, and 1.4 mM KH_2PO_4 (pH 7.4)]; TES, 10 mM *N*-tris(hydroxymethyl)methyl-2-aminoethanesulfonic acid with 100 mM NaCl and 40 mM KCl at pH 7.4; Tris-HCl, 10 mM Tris-HCl buffer with 100 mM NaCl and 40 mM KCl at pH 7.4.

10.1021/bi052321z CCC: $33.50
Published on Web 04/06/2006

insight into the mechanism of statherin function on the hydroxyapatite surface.

MATERIALS AND METHODS

Hydroxyapatite Preparation. Hydroxyapatite seed crystals with a density of 0.032 g/mL were generously provided by A. Campbell (Battelle Pacific Northwest National Laboratory, Richland, WA) (*31*). X-ray powder diffraction (Phillips) confirmed the formation of HAP and the absence of other unwanted calcium phosphate phases. BET (Quantachrom) measurements showed a specific surface area of 53 m^2/g. The calcium (Ca) to phosphorus (P) ratio, measured by inductively coupled ion plasma (ICP) spectroscopy, was determined to be 1.67. Crystal morphology as determined by electron microscopy (using scanning and transmission modes) was as expected for hydroxyapatite. Before usage, the HAP suspension was centrifuged and the pellet washed twice with the working buffer.

Protein Synthesis. Statherin was synthesized using standard Fmoc solid-phase synthesis. Fmoc-protected amino acids, including protected phosphoserine {Fmoc-Ser[PO(OBzl)-OH]-OH} and the preloaded resin Fmoc-Phe-Novasyn-TGA (0.21 mmol/g substitution), were purchased from Novabiochem. The synthesis was carried out on an automated Rainin PS3 peptide synthesizer. All amino acids were double coupled with a 4-fold excess of protected amino acids. Due to coupling difficulties, the phosphoserines were used with a 5-fold excess and an extended coupling time. Coupling was performed using the activator 2-(1*H*-benzotriazol-1-yl)-1,1,3,3-tetramethyluronium hexafluorophosphate (HBTU) in 0.4 M *N*-methylmorpholine in DMF.

The protein was cleaved from the resin and deprotected in 95% trifluoroacetic acid, 2.5% triisopropylsilane, and 2.5% water. After the reaction was allowed to proceed with gentle mixing for 2 h, the solution was filtered and concentrated to approximately 5 mL. The trifluoroacetic acid/protein solution was then added dropwise to cold *tert*-butyl methyl ether. Crude precipitate was washed and dried under nitrogen.

Protein Purification and Characterization. Protein purification was performed on a 10 mm (diameter) × 100 mm (length), 7.9 mL, POROS HQ/M strong anion exchange column plumbed to a BioCAD SPRINT perfusion chromatography system. The mobile buffer consisted of 50 mM Tris-HCl at pH 8.5 (A), buffer A with 0.5 M NaCl (B), and acetonitrile (C), and the latter was kept fixed at 30% to maintain protein solubility. The column was equilibrated with 3 column volumes of 70% buffer A and 30% acetonitrile. The crude protein was dissolved in 30% acetonitrile in buffer A at a final concentration of 10 mg/mL, and a volume of 3 mL was injected through the sample loader into a 4 mL loop at a time. A linear gradient from 0 to 70% B in 14.7 column volumes was used to elute the protein at a flow rate of 3 mL/min. UV absorption was detected at a wavelength of 280 nm. Fractions eluted at 35% buffer B and containing the pure protein were pooled and concentrated using a Centriplus centrifugal filter unit (3 kDa molecular mass cutoff). When this purity was not sufficient, the protein was further purified on a Varian HPLC system equipped with an Altima C4 column using a gradient of acetonitrile in water (both with 0.1% trifluoroacetic acid) and the protein eluted at 42% acetonitrile. The pure concentrated protein was then subjected to buffer exchange on Sephadex G-25 PD-10 column that was pre-equilibrated in the buffer used in the specific experiment. The purity of statherin (~95%) was established using liquid chromatography−electrospray ionization mass spectrometry, and the concentration was determined from amino acid analysis.

Circular Dichroism. CD experiments were carried out on an AVIV 62DS spectropolarimeter. A quartz cell with a path length of 0.1 cm was used with a statherin concentration of 0.2 mM in phosphate buffer (PB) with the following composition: 100 mM NaCl, 40 mM KCl, 4.3 mM Na_2HPO_4, and 1.4 mM KH_2PO_4 (pH 7.4). Spectra were recorded between 250 and 195 nm at 0.5 nm steps with a time constant of 5 s at 25 °C. The resultant spectrum was similar to the one previously reported for statherin, with a characteristic broad negative signal minimum between 197 and 210 nm (*8*, *9*). The temperature dependence of the CD signal at 210 nm was detected from 5 to 37 °C at a rate of 1 °C/min. No change in the signal was observed over this temperature range.

Differential Scanning Calorimetry. DSC experiments were performed by V. Frasca from Microcal, LLC, on a VP-DSC system. The instrument was set in passive mode. The statherin solution (0.3 mM in PB) was heated from 10 to 130 °C at a rate of 1 °C/min. The resultant DSC trace was the same as the reference scan (PB only), and no transition was observed over the whole temperature range.

Isothermal Titration Calorimetry. ITC experiments were carried out on a VP-ITC system (Microcal, LLC) at temperatures from 15 to 37 °C. Statherin appears to be stable over that temperature range, as observed from the absence of CD as well as DSC transition at these temperatures (data not shown). Unless otherwise noted, all experiments were performed in PB (pH 7.4), with both protein and mineral initially in the same buffer. To study the effects of protonation on statherin−HAP interactions, additional calorimetric experiments were performed in 10 mM Tris-HCl with 100 mM NaCl and 40 mM KCl (pH 7.4) or in 10 mM TES with 100 mM NaCl and 40 mM KCl (pH 7.4).

For all experiments, statherin (0.16 mM) was injected in 25 μL increments into the isothermal calorimetry cell (1.42 mL) prefilled with a HAP suspension in buffer (2 mg/mL). The protein concentration was chosen to achieve sufficiently high heat signals with a minimum enthalpy of dilution. The HAP concentration was chosen to allow as many data points as possible to be recorded, until saturation was reached, within a single experiment. This is dictated by the maximum volume available (250 μL) in the ITC's injection syringe. To minimize the error associated with diffusion from the syringe during baseline equilibration, the first injection was only 5 μL, and the associated small heat was not included in the data analysis. A 4 min interval was allowed between injections for equilibration of the adsorbed protein; this period was sufficient for return of the heat signal to baseline between injections.

A blank experiment in which statherin was injected into a HAP suspension's supernatant (minus the HAP) was carried out and was used to correct the data due to dilution. The blank heat change was found to be comparable to the heat change observed in the last injections and was used as a measure of the background heat signal. This background was subtracted from the measured heats, and the corrected heats

were divided by the number of moles of the injectant and analyzed using the equations described below (*32*).

Equations Used in Isothermal Titration Calorimetry Data Analysis. In a typical ITC experiment, the equilibrium binding constant of one set of binding sites can be expressed as

$$K = \frac{\theta}{(1-\theta)[\mathrm{C}]} \tag{1}$$

where [C] is the equilibrium concentration of protein in solution and θ is the fraction of receptor sites that are occupied by bound protein.

The total concentration of the protein in the ITC cell, C_t, is given by the sum of contributions from the free and bound protein:

$$C_t = [\mathrm{C}] + n\theta M_t \tag{2}$$

where n is the binding stoichiometry and M_t is the molar concentration of the protein's receptor in the ITC cell. Here, we describe adsorption of a protein molecule onto a solid surface and as such must use a modified expression. Therefore, we used the binding isotherm results (presented below) to obtain the maximum (saturation) number of moles of sites accessible to the protein on the HAP surface per unit mass of HAP and multiplied this by the mass of HAP in the ITC cell to obtain M_t', the molar concentration of adsorption sites on the mineral surface per unit volume in the ITC cell:

$$M_t' = N_{\max}\frac{\text{moles}}{m^2}\mathrm{SA}\frac{m^2}{gr}D\frac{gr}{L} \tag{3}$$

where $N_{\max}$ is the maximum number of binding sites per unit surface area, SA is the specific surface area of the HAP (per gram) obtained from BET measurements, and D is the amount of HAP placed in the ITC cell (in grams) per unit volume of the ITC cell. Thus, M_t' replaces the product nM_t in eq 2, which thus becomes

$$C_t = [\mathrm{C}] + \theta M_t' \tag{4}$$

where θ is now the fraction of surface sites occupied by the protein. It is notable that the molarities of the different terms in eq 4 are calculated differently. [C] is calculated per unit of liquid volume, whereas the other terms are moles per unit volume of the whole ITC cell (liquid and solid). However, since the solid mineral occupies only ~3% of the ITC cell volume, we have neglected its volume in eq 4.

Combining eqs 1 and 4 gives

$$\theta^2 - \theta\left(1 + \frac{C_t}{M_t'} + \frac{1}{KM_t'}\right) + \frac{C_t}{M_t'} = 0 \tag{5}$$

As shown below, only a small fraction of the statherin molecules which adsorb on HAP display a heat of adsorption that can be measured via calorimetry. We have attributed this to the presence of two different types of sites on the surface: A sites which are populated first and have a measurable molar enthalpy of adsorption, ΔH, which is independent of coverage and B sites which have no measurable heat of adsorption. The total measured heat content (Q) of the solution contained in an ITC cell due to adsorption as a function of the fractional population of A sites, θ, is given by

$$Q = \theta\alpha M_t'\Delta H V_0 \tag{6}$$

where α is the fraction of all sites that are A-type sites and V_0 is the working ITC cell volume.

If we assume that the A and B sites populate independently with simple Langmuir adsorption isotherms and that the A site population nearly reaches saturation before significant population of the B sites, then the fractional coverage of A will still be well approximated by eq 5 if we simply replace M_t' with the product $\alpha M_t'$ (the factor α plays the same role mathematically as the stoichiometry in normal ITC analysis but has a very different physical meaning).

Solving the quadratic equation for θ and then substituting it into eq 6 gives

$$Q = \frac{\alpha M_t'\Delta H V_0}{2}\left[1 + \frac{C_t}{\alpha M_t'} + \frac{1}{K\alpha M_t'} - \sqrt{\left(1 + \frac{C_t}{\alpha M_t'} + \frac{1}{K\alpha M_t'}\right)^2 - \frac{4C_t}{\alpha M_t'}}\right] \tag{7}$$

The change in heat content from the completion of injection $i-1$ to completion of injection i is

$$\Delta Q(i) = Q(i) - Q(i-1) + \frac{\mathrm{d}V_i}{V_0}\left[\frac{Q(i) + Q(i-1)}{2}\right] \tag{8}$$

where $\mathrm{d}V_i$ is the injection volume. The last term corrects for heat loss by displacement of liquid out of the ITC cell, where $Q(i)$ is the heat content after injection i.

If the values of K, ΔH, and α were known, the value of $Q(i)$ could be calculated at the end of each injection using eqs 7 and 8. Instead, by guessing initial values for K, ΔH, and α and fitting the experimental data, $Q(i)$, to eq 7 by an iterative procedure, we determined the best-fit values for K, ΔH, and α.

The critical parameter which determines the shape of the binding isotherm is the unitless constant c which is given by the relationship $c = \alpha M_t' K$. For an accurate determination of the binding constant, the c value should ideally be between 1 and 1000 (*32*). The calculated c values for the titration of HAP crystals with statherin in phosphate buffer at 15, 20, 25, 30, and 37 °C are 6, 13, 132, 103, and 101, respectively, and for the titration in Tris and TES buffers at 25 °C are 3.4 and 5, respectively.

Equilibrium Adsorption Binding Isotherm. In adsorption experiments, known amounts of statherin (5−100 μM) in PB were equilibrated for 4 h with a HAP suspension at either 24 or 37 °C. Samples were prepared in duplicates for each protein concentration. After incubation, the protein concentrations in the supernatant were determined using a Micro BCA protein assay reagent kit (Pierce) recording the absorbance at 562 nm on a safire^2 TECAN plate reader. The instrument was calibrated by triplicate measurements of statherin samples with known variable concentrations. The amount of protein on the HAP surface was determined by subtraction of the measured quantity from the initially added amount. Matlab function "FMINS", which minimizes a

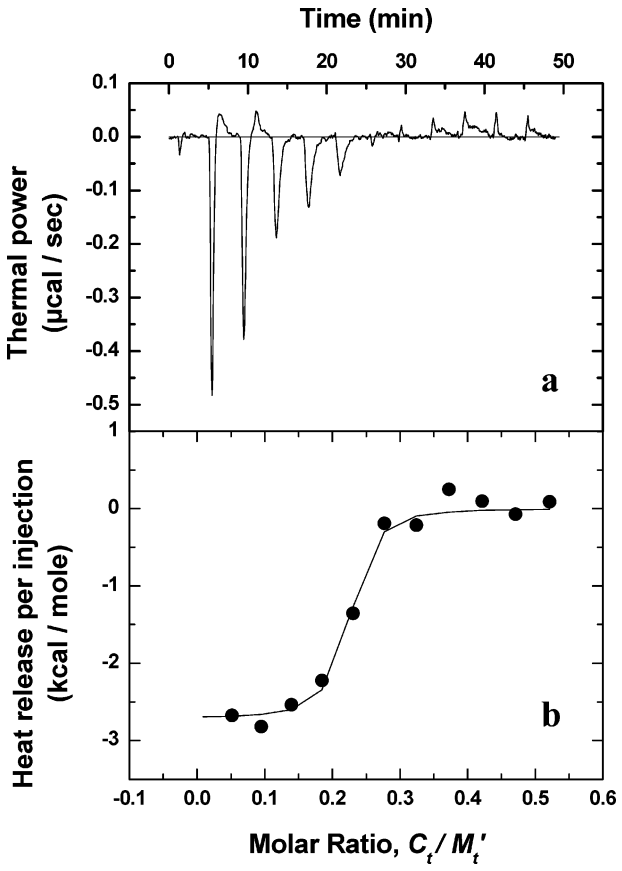

FIGURE 1: (a) ITC profile of the titration of HAP (2 mg/mL) with statherin (0.16 mM) performed at 25 °C in PB. (b) Titration curve corrected for the heat of dilution and depicted as a function of the molar ratio between the total injected statherin concentration, C_t, and the molar concentration of HAP adsorption sites, M_t'. Data points were fit as described in Materials and Methods.

function of several variables using the Nelder−Mead simplex method (*33*), was used to fit the experimental data to various models (described below).

RESULTS

Isothermal Titration Calorimetry (ITC). The thermodynamic adsorption parameters were derived from ITC measurements where an initial sample of HAP crystals (2 mg/mL) in the ITC cell was titrated with repeated injections of statherin (0.16 mM). Figure 1 depicts a typical isothermal titration curve of adsorption, in this case at 25 °C. Extending the titration with 12 additional injections resulted in no change to the measured heat. The results shown are representative of multiple experiments. Repeated experiments with double the amount of HAP in the ITC cell (4 mg/mL) and a statherin concentration of 0.32 mM in the syringe gave a similar titration curve with K and ΔH values that are within experimental error (Table 1).

Figure 1a shows the raw data corresponding to the apparent heats of adsorption depicted in units of microcalories per second versus time. The heat change in each injection was corrected for the heat of dilution and divided by the number of moles of injected statherin. The resulting values of the measured heat of reaction per mole of injected statherin are plotted as a function of the ratio of total injected statherin concentration, C_t, to the maximal concentration of statherin sites on HAP, M_t', as shown in Figure 1b. The adsorption of

Table 1: Temperature Dependence of the Apparent Thermodynamic Parameters for Adsorption of Statherin onto HAP in PB, Obtained from ITC

temp (°C)	α	ΔH (kcal/mol)	$T\Delta S°$ (kcal/mol)	$\Delta G°$ (kcal/mol)	K (M^{-1})
15	0.21	-5.4 ± 0.4	2.1 ± 0.3	-7.4 ± 0.1	$(4.3 \pm 0.8) \times 10^5$
20	0.18	-4.0 ± 0.4	4.1 ± 0.2	-8.1 ± 0.2	$(1.1 \pm 0.4) \times 10^6$
25	0.21	-2.7 ± 0.1	6.8 ± 0.2	-9.5 ± 0.4	$(9.5 \pm 5.8) \times 10^6$
30	0.13	-1.8 ± 0.2	8.0 ± 0.2	-9.8 ± 0.3	$(1.2 \pm 0.6) \times 10^7$
37	0.11	-1.6 ± 0.4	8.5 ± 0.3	-10.1 ± 0.5	$(1.4 \pm 1.0) \times 10^7$

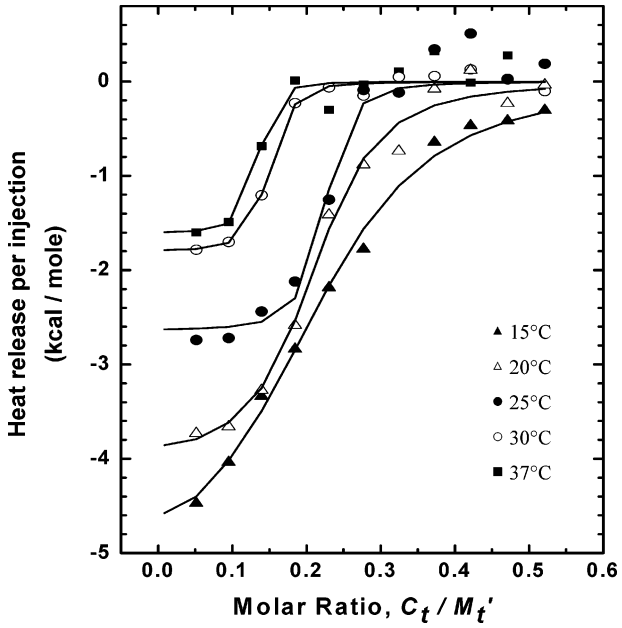

FIGURE 2: Titration curves corrected for the heat of dilution obtained for the titration of HAP (2 mg/mL) with statherin (0.16 mM) performed at 15 (▲), 20 (△), 25 (●), 30 (○), and 37 °C (■) in PB. Data points were fit as described in Materials and Methods.

statherin is initially exothermic but has a low apparent heat of adsorption (∼3 kcal/mol). However, the enthalpy of adsorption drops to around zero after only enough statherin was injected to occupy ∼30% of the sites on the HAP as determined from the binding isotherm. This is because only a small fraction of the sites that bind statherin do so with a measurable heat of adsorption (see below).

Titration curves for adsorption of statherin onto HAP were measured at other temperatures between 15 and 37 °C, as shown in Figure 2. At each temperature, the equilibrium association constant, K, the apparent enthalpy change of adsorption, ΔH_{app}, and the fraction of protein adsorption sites that have this enthalpy of adsorption, α, were directly obtained from the best fit of the calorimetry data to eq 7 using the iterative procedure described above. The apparent standard Gibbs free energy change ($\Delta G°_{app}$) and the standard entropy change ($\Delta S°_{app}$) were calculated from the equalities $\Delta G° = -RT \ln K = \Delta H - T\Delta S°$. The results are summarized in Table 1. The apparent enthalpy of adsorption increases with temperature from −5.4 to −1.6 kcal/mol, while the fraction of sites that have this heat of adsorption varies less, decreasing from 0.21 to 0.11. The standard free energy of adsorption also stays relatively constant, but the entropy of adsorption increases 4-fold between 15 and 37 °C.

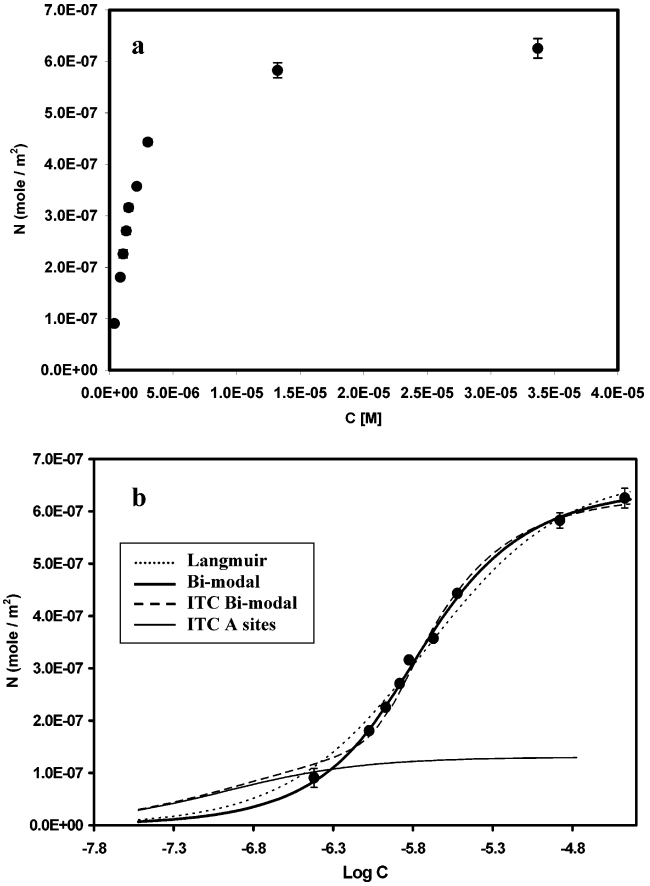

FIGURE 3: (a) Adsorption isotherm data for the binding of statherin to HAP (2 mg/mL at 1.42 mL) at 24 °C. (b) The same adsorption data plotted vs the log of the equilibrium concentration. The dotted line is the best fit to the Langmuir model. The solid bold line is the best fit to the bimodal model where 21% of the protein molecules bind according to a Langmuir model and 79% according to an attractive model, as given in eqs 10−12. The dashed line is that same fit to the bimodal model but while applying α and K_A values obtained from the ITC measurements (Table 2, ITC bimodal fit). The solid thin line represents the generated adsorption isotherm to A sites applying α and K_A values from ITC at 25 °C (Table 1).

Equilibrium Adsorption Isotherm Measurements. The equilibrium isotherm for adsorption of statherin onto HAP at 24 °C is shown in Figure 3a as the number of moles adsorbed per unit of surface area, N, versus the equilibrium concentration of free statherin in solution, [C], with the points collected sequentially with an increase in [C], allowing 4 h for equilibration at each concentration. These data are replotted in Figure 3b as N versus log[C].

A simple first-order Langmuir adsorption isotherm with independent binding sites predicts that the surface coverage should vary with concentration as

$$N = \frac{KN_{max}[C]}{1 + K[C]} \tag{9a}$$

or

$$\theta = \frac{K[C]}{1 + K[C]} \tag{9b}$$

where N_{max} is the maximum number of binding sites per unit surface area, K is the equilibrium binding constant, and θ ($=N/N_{max}$) is the fractional coverage. This is a simple rearrangement of eq 1.

The data in Figure 3 are reasonably well fit by this simple first-order Langmuir adsorption isotherm, as shown by the dotted line, with the following best-fit values: $K = (8.0 \pm 1.0) \times 10^5$ M^{-1} and $N_{max} = (6.7 \pm 0.3) \times 10^{-7}$ mol/m^2. Binding isotherms carried out with 1 and 2 mg/mL HAP gave rise to similar N_{max} and K values. The average values obtained at the various experiments are given in Table 2 with the associated errors. Those values are within the same order of magnitude as those previously reported (*4*), with minor differences that may be attributed to variations under solution conditions.

As noted above, this N_{max} value was used to calculate M_t' with eq 3. This M_t' value is much larger than the concentration of sites that have a measurable heat of adsorption according to the ITC data, as reflected in the low values for α (0.11−0.21) in Table 1. That is, the calorimetric results do not coincide with the binding isotherm data in that the latter gives a much higher saturation coverage when both are independently analyzed assuming a first-order Langmuir adsorption isotherm. Also, the ITC data give an equilibrium constant that is more than 10-fold larger than the isotherm data. A very similar equilibrium adsorption isotherm was also measured at 37 °C (Figure 4a). The parameters of the fit to the simple Langmuir model of eq 9 are listed in Table 2. The saturation coverage and equilibrium constant are almost independent of temperature.

The calorimetric results were combined with the equilibrium adsorption isotherm data to estimate the enthalpy associated with adsorption versus fractional coverage of surface sites, N/N_{max}, at 25 and 37 °C. The results are shown in Figure 5. The x-axis conversion from moles injected to moles adsorbed was made using the equilibrium adsorption isotherm (Figure 3), with the assumption that equilibrium was reached after each calorimetry injection. From the figure, it is clearly seen that at low coverage the adsorption is driven by an exothermic enthalpy but that the heat of adsorption drops to near zero by ∼40% saturation at 25 °C and only ∼20% saturation at 37 °C.

We interpret these results and those in Table 1 as indicating that there are two types of sites on the HAP: A-type sites with a measurable heat of adsorption and a larger equilibrium constant which populate first but which account for only ∼16 ± 5% of the total sites and B-type sites with no measurable heat of adsorption and a far weaker binding constant. Such a two-state model is not surprising, since it is well-known in the literature that adsorption of protein onto surfaces is not a single process (*27*, *34*−*36*). Note that the B sites either have a heat of adsorption that is really negligible or, since the calorimeter is insensitive to heat that is exchanged too slowly, may also have a substantial heat of adsorption but simply populate too slowly to give a measurable heat.

From Table 1, it is clear that entropy makes the dominant contribution to the free energy of adsorption even at low coverage where adsorption in exothermic. Adsorption beyond ∼30% saturation appears to be due entirely to the increase in entropy, unless any heat of adsorption is too slowly delivered to measure.

The ITC experiment occurs on a much faster time scale (4 min per injection) compared to the isotherm data of Figure 3 (hours). To verify that the extent of adsorption at the end

Table 2: Parameters for Adsorption of Statherin onto HAP Calculated from Best Fits of the Langmuir (eqs 1 and 9) and Bimodal (eqs 10−12) Equilibrium Binding Isotherm Models to the Measured Equilibrium Binding Isotherms at 24 and 37 °C[a]

	Langmuir		bimodal				
temp (°C)	N_{max} ($\times 10^{-7}$ mol/m^2)	K ($\times 10^5$ M^{-1})	N_{max} ($\times 10^{-7}$ mol/m^2)	α	K_A ($\times 10^5$ M^{-1})	β ($\times 10^5$ M^{-1})	K_B ($\times 10^5$ M^{-1})
24	6.7 ± 0.3	8.0 ± 1.0	6.4 ± 0.2	0.21	7.6 ± 1.0	6.6 ± 3.0	2.4 ± 0.5
24 (ITC)			6.3 ± 0.2	0.21 (ITC)	95 ± 58 (ITC)	8.5 ± 4.0	0.5 ± 0.2
37	6.3 ± 0.3	7.4 ± 0.9	6.0 ± 0.2	0.11	9.0 ± 2.0	13 ± 3.0	2.6 ± 0.5
37 (ITC)			6.0 ± 0.2	0.11 (ITC)	140 ± 100 (ITC)	13 ± 3.0	1.4 ± 0.5

[a] ITC is a bimodal fit applying α and K_A values obtained from ITC (Table 1) at the closest temperature.

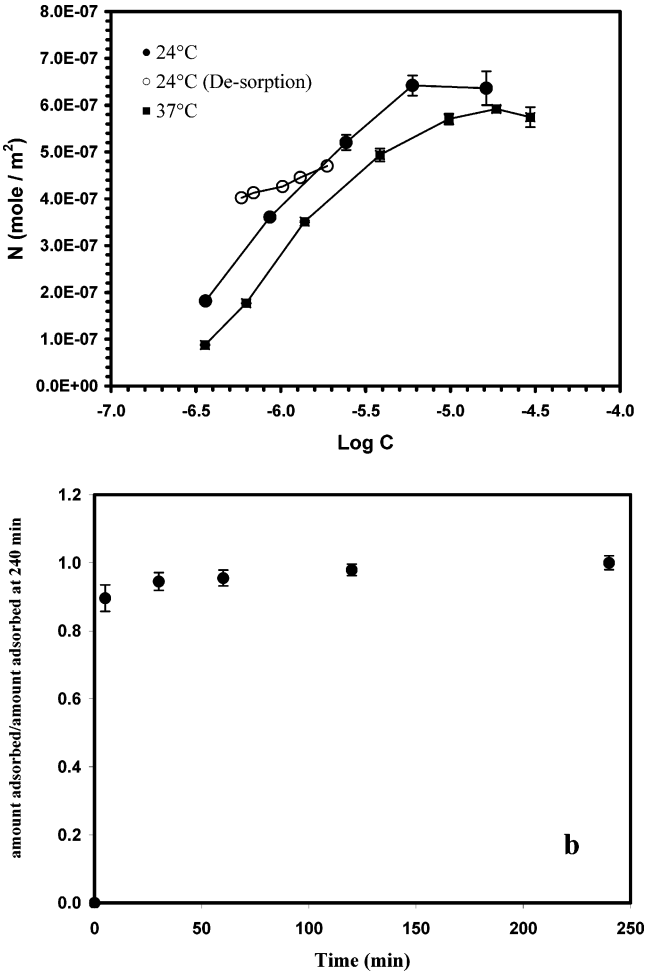

FIGURE 4: (a) (■) Adsorption isotherm for statherin and HAP (1 mg/mL) performed at 37 °C and plotted vs the log of the equilibrium concentration. Adsorption (●) and desorption (○) isotherms for statherin and HAP (1 mg/mL) at 24 °C. Desorption data were collected with an initial coverage of 5.2×10^{-7} mol/m^2. (b) Time course of the adsorption of statherin (5.2×10^{-7} mol/m^2) onto HAP (1 mg/mL) at 24 °C.

of the ITC experiment reaches its equilibrium value, the contents of the sample cell were promptly recovered and centrifuged at the end of titration. The protein concentration in the supernatant was then determined by a BCA assay. In all experiments for statherin injections up to a C_t/M_t' of 0.52 (end of titration, Figures 1 and 2), more than 90% of the total injected statherin was adsorbed onto the mineral as expected from the equilibrium adsorption isotherm (Figure 3) and the (even larger) equilibrium constant determined from the ITC data (Table 1).

We also fit the binding isotherm data of Figure 3 with a simple model involving two first-order Langmuir-type adsorption sites, each populated independently and with

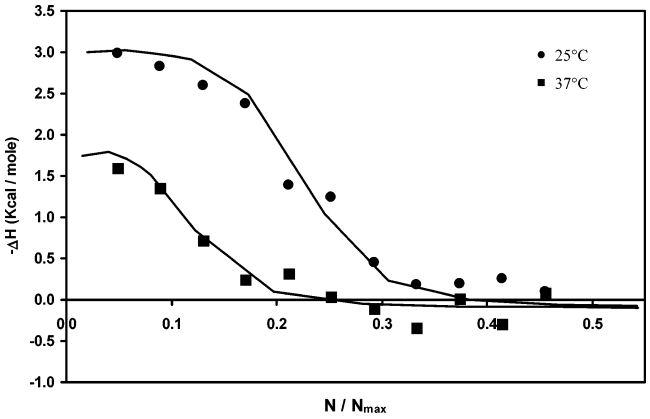

FIGURE 5: Plot of the heat of adsorption ($-\Delta H$ per mole of adsorbed protein) vs coverage at 25 (●) and 37 °C (■) (representative experiments). The data were fit using eqs 13 and 14 and applying the α and K_A values from the ITC for A sites (Table 1) and the rest of the parameters from the bimodal fit to the isotherm data (Table 2, ITC bimodal fit).

different equilibrium constants. In this case, the overall coverage is expressed as the sum of the two processes and eq 9b becomes

$$\theta_{total} = \alpha\theta_A + (1-\alpha)\theta_B = \alpha\frac{K_A[C]}{1+K_A[C]} + (1-\alpha)\frac{K_B[C]}{1+K_B[C]} \quad (10)$$

where α is the fraction of sites that are A-type.

Fitting the binding isotherm data in Figure 3 to this model gave similar values for K_A and K_B with no noticeably better quality fit than a single-site model. However, the data could be fit better by such a model if we assumed that the equilibrium constant for the B sites, K_B, increases with increasing coverage of B sites. In this case, K_B must be treated as a function of θ and therefore becomes K_B':

$$K_B' = K_B + \beta\theta = \frac{\theta_B}{(1-\theta_B)[C]} + \beta\theta_B \quad (11)$$

where β is a correction to the equilibrium constant that accounts for attractive interactions between the assembled molecules. To express the coverage dependence on [C] in the process of adsorption to site B, eq 11 can be rearranged as follows:

$$\theta_B = \frac{1}{2\beta[C]}\left[\beta[C] - K_B'[C] - 1 \pm \sqrt{(1+K_B'[C]-\beta[C])^2 + 4K_B'\beta[C]^2}\right] \quad (12)$$

We then simply substitute the expression for θ_B in eq 10

with the one in eq 12. Figure 3b shows that such a model fits the isotherm very well (solid bold line). The calculated adsorption parameters are summarized in Table 2.

The K_A value in Table 2 is 10-fold smaller than the equilibrium constants determined from ITC fitting at similar temperatures (Table 1). This is probably because of the very low population of A-type sites that have a measurable heat of adsorption (~16% of the total), coupled with the fact that the adsorption isotherms have no data points below this coverage. This renders their fits very insensitive to the parameters that define the A-type sites. For example, if the much more populous B sites have some heterogeneity, it is likely that the two different types of sites that result from fitting the isotherm data correspond to subpopulations of B sites, missing the contribution from A sites almost entirely.

For the purpose of comparison between the equilibrium binding isotherm and the ITC experiment, we have generated a putative binding isotherm of process A by applying K_A and α values that were obtained from the ITC measurement. Figure 3b depicts the measured binding isotherm (solid data points) and the simulation for process A alone (solid thin line) using the parameters determined for it by fitting the ITC data at the closest temperature (25 °C), listed in Table 1. It is notable that process A reaches saturation rapidly and its contribution to the binding isotherm is at the early stages of the adsorption where the equilibrium concentrations are low. Because of a lack of sensitivity of the BCA assay at those low protein concentrations, we could not conduct a binding isotherm mimicking the ITC experiment.

Figure 3b also displays a fit of the binding isotherm data using another bimodal model in which both the K_A and α values were assumed to be those determined from the best fit to the ITC measurements in Table 1 (dashed line). The other three parameters were determined to give the best fit to the data and are listed in Table 2. We call this the "ITC bimodal model". Given the data statistics, there is not a significant difference in the quality of this fit and that of the bimodal fit given above that had more adjustable parameters. Both give good fits to the data. They differ strongly only below 15% saturation, where there are no data. This new fit represents the best bimodal model that is most consistent with all of the data (i.e., both the ITC data and the adsorption isotherm). The binding isotherm at 37 °C was similarly analyzed, and the recovered parameters are given in Table 2.

To isolate the coverage change in process A relative to the total coverage in eq 10, one can write the differential change in process A versus the total coverage:

$$\mathrm{d}\left(\frac{N_A/N_{max}}{N/N_{max}}\right) = \alpha\left(\frac{\mathrm{d}\theta_A}{\mathrm{d}\theta_{total}}\right) \tag{13}$$

This is advantageous when we choose to follow exclusive contributions due to process A, which involves an enthalpy change, while process B involves no change in heat. This function is utilized to extract the actual binding enthalpy change, ΔH_{act}, of process A from measurement of the apparent enthalpy change, ΔH_{app}, with coverage as follows:

$$\Delta H_{app}(N/N_{max}) = \Delta H_{act}\frac{\mathrm{d}(N_A/N_{max})}{\mathrm{d}(N/N_{max})} \tag{14}$$

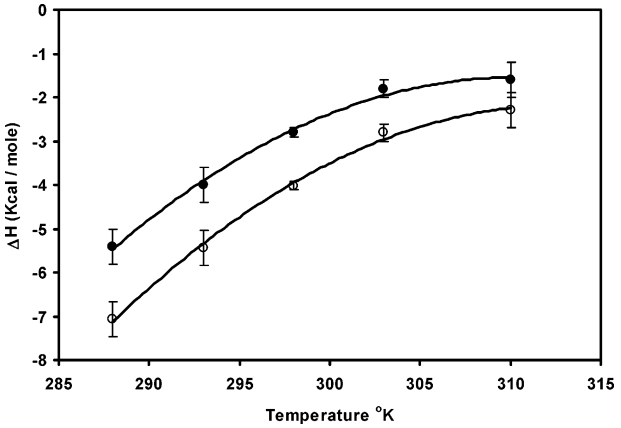

FIGURE 6: Adsorption enthalpy, ΔH, apparent (●) and corrected due to ionization (○), as a function of temperature. Solid lines are best fit to eq 15 with γ values of -15.86 ± 0.06 and -15.93 ± 0.06 cal K^{-2} mol^{-1} for apparent and corrected, respectively.

Table 3: Temperature Dependence of the Enthalpy and Heat Capacity Change for Adsorption of Statherin onto HAP[a]

temp (°C)	ΔH_{app} (kcal/mol)	ΔC_{papp} (cal mol^{-1} K^{-1})	ΔH_{ass} (kcal/mol)	ΔC_{pass} (cal mol^{-1} K^{-1})
15	-5.4 ± 0.4	352 ± 25	-7.1 ± 0.4	397 ± 28
20	-4.0 ± 0.4	273 ± 27	-5.4 ± 0.4	317 ± 31
25	-2.7 ± 0.1	194 ± 7	-4.0 ± 0.1	237 ± 8
30	-1.8 ± 0.2	115 ± 13	-2.8 ± 0.2	158 ± 17
37	-1.6 ± 0.4	4 ± 1	-2.3 ± 0.4	47 ± 12

[a] app, apparent value; ass, (association) value corrected due to buffer ionization.

The experimental data in Figure 5 were fit with the above equation applying the K_A value from the ITC for A sites (Table 1) and the rest of the parameters from the ITC bimodal model to the isotherm data (Table 2). The resulting values of ΔH_{act} from this fitting are −3.3 and −2.1 kcal/mol for 25 and 37 °C, respectively. Those values are slightly higher than the ITC ΔH_{app} values (Table 1). This is because a few B-type sites are also being populated during the ITC injections so that the A-type sites correspond to only ~80% of the total adsorption during ITC in this model (see Figure 3b). To give the same amount of heat, the adsorption heat per mole of A-type adsorbate must then be scaled up by 25%.

Effect of Temperature on the Adsorption Enthalpy. The change in the reaction enthalpy with temperature defines the reaction's heat capacity change, ΔC_p. Its value for adsorption of statherin onto A sites of HAP was estimated by plotting the adsorption enthalpies measured by ITC at different temperatures [Figure 6(●)]. The change in adsorption enthalpy with temperature can be described by

$$\Delta H(T) = \Delta H_r + (\Delta C_{pr} - \gamma T_r)(T - T_r) + \frac{1}{2}\gamma(T^2 - T_r^2) \tag{15}$$

where ΔH_r, ΔC_{pr}, and T_r are the enthalpy change, heat capacity change, and temperature, respectively, defined at a relative fixed temperature and γ defines the change in heat capacity with temperature. Fitting the data in Figure 6 to eq 15 resulted in a γ value of -15.86 ± 0.06 cal K^{-2} mol^{-1}. The calculated apparent ΔC_p values at each temperature are given in Table 3. These values, of course, apply only to the A-type sites of HAP.

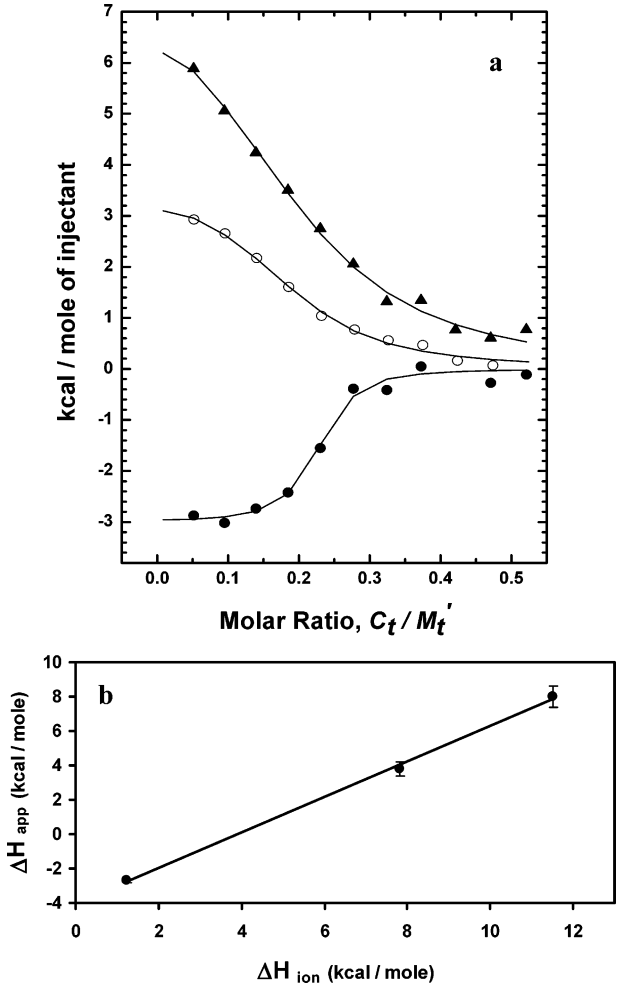

FIGURE 7: (a) Titration curve corrected for the heat of dilution obtained for the titration of HAP (2 mg/mL) with statherin (0.16 mM) at pH 7.4 and 25 °C in PB (●), TES (○), and Tris-HCl (▲). Data points were fit as described in Materials and Methods. (b) ΔH_{app} vs ΔH_{ion} at pH 7.4 and 25 °C. Ionization enthalpy changes used for the buffers were 1.22 kcal/mol for PB, 7.83 kcal/mol for TES, and 11.51 kcal/mol for Tris-HCl (*38*, *39*). The solid line is the best fit to eq 16.

Effect of Buffer Ionization on the Adsorption Process. Often, the binding event is not an isolated protein−mineral interaction but involves several underlying events such as water association or dissociation, ionization of the protein or mineral, binding of mediating molecules, etc. (*27*). The enthalpy recorded in a calorimetry experiment will reflect the sum of heats from the associated events. To facilitate binding, residues at the interface may be protonated or deprotonated, resulting in exchange of protons with the buffer. Under such circumstances, the detected heat change is dependent on the buffer ionization enthalpy. By performing identical titration experiments in additional buffers with different enthalpies of ionization (once again both the protein in the syringe and the mineral in the ITC cell are in the same buffer), we are able to determine whether protonation or deprotonation events occur during the adsorption process (*37*, *38*). Figure 7a compares the titration curves obtained for adsorption of statherin onto HAP in PB, TES, and Tris-HCl buffers at pH 7.4 and 25 °C. The apparent thermodynamic parameters are summarized in Table 4. From the table, it is notable that the adsorption process in TES and Tris-HCl is exclusively driven by entropy.

Table 4: Apparent Thermodynamic Parameters for Adsorption of Statherin onto HAP Obtained from ITC at 25 °C in Three Buffer Systems at pH 7.4

buffer	α	ΔH (kcal/mol)	$T\Delta S°$ (kcal/mol)	$\Delta G°$ (kcal/mol)	K (M^{-1})
PB	0.21	-2.7 ± 0.1	6.8 ± 0.2	-9.5 ± 0.4	$(9.5 \pm 5.8) \times 10^6$
TES	0.18	3.8 ± 0.4	11.4 ± 0.4	-7.6 ± 0.2	$(3.9 \pm 1.2) \times 10^5$
Tris-HCl	0.19	8.0 ± 0.6	15.4 ± 0.4	-7.4 ± 0.1	$(2.7 \pm 0.5) \times 10^5$

The apparent enthalpy change measured in PB is exothermic (2.7 ± 0.1 kcal/mol), whereas in TES and Tris-HCl, it is endothermic (3.8 ± 0.4 and 8.0 ± 0.6 kcal/mol, respectively). The apparent enthalpy comprises the binding enthalpy change due to association (ΔH_{ass}) and the buffer heat of ionization (ΔH_{ion}) according to

$$\Delta H_{app} = \Delta H_{ass} + n_{H^+}\Delta H_{ion} \quad (16)$$

where n_{H^+} is the number of protons involved in the interaction.

A plot of the calorimetric enthalpy versus the buffer ionization enthalpy (Figure 7b) yielded an n_{H^+} value of 1.03 ± 0.01 and an association enthalpy of -4.07 ± 0.01 kcal/mol. The calculated positive value of n_{H^+} for adsorption of statherin onto A sites of HAP indicates that their interaction is mediated by a net uptake of proton from the buffer.

The ΔH_{ass} at the various temperatures was calculated using a ΔC_p value of -44 cal K^{-1} mol^{-1} for PB deprotonation (*39*) and under the assumption that the n_{H^+} value is constant in the temperature range that was studied. The calculated ΔH_{ass} data versus temperature are plotted in Figure 6 (○) and reported in Table 3. The heat capacity change, corrected for buffer ionization (ΔC_{pass}) as a function of temperature, is derived from fitting $\Delta H_{ass}(T)$ using eq 15. Values for $\Delta C_{pass}(T)$ are given in Table 3. The resulting γ value corrected due to buffer ionization is similar to the apparent γ value (-15.93 ± 0.06 and -15.86 ± 0.06 cal K^{-2} mol^{-1}, respectively).

Reversibility of the Adsorption Process. The analysis of the ITC as well as the equilibrium binding isotherm requires reversibility of the adsorption process. According to prior literature, statherin adsorbs onto HAP in a reversible fashion (*28*). To test this, we measured N versus [C] also in the reverse direction, by desorption of statherin from the HAP surface, at the same temperature and HAP concentration. To do this, a nearly saturated HAP sample was first prepared by mixing the protein with HAP (1 mg/mL) for 4 h, resulting in a high initial statherin coverage of 5.2×10^{-7} mol/m^2. The supernatant was removed, and the solid complex was diluted and mixed with fresh buffer, allowing 2.5 h for equilibration. This process of removing the supernatant, diluting in buffer, and re-equilibrating was repeated five times. The amounts of free and bound protein were determined as usual following each equilibration. The resulting desorption data points (○) shown in Figure 4a are superimposed on the data points for the adsorption isotherm (●). The desorption data fall within the error range of that binding curve, thereby supporting a model wherein adsorption of statherin onto HAP is reversible.

Reliance of the ITC and Binding Isotherm Measurements. The ITC and binding isotherm experiments are generally carried out differently. Here, the titration experiment moni-

tored the accumulated effect of protein additions on adsorption with an interval of 4 min between additions. The isotherm, on the other hand, was measured from a set of separate samples with an increasing protein concentration and a fixed adsorbent concentration that were equilibrated for 4 h. To determine whether adequate adsorption is attained in each ITC injection, we measured the amount of adsorbed protein as a function of time. Figure 4b shows that the adsorption of statherin onto HAP is rapid at 24 °C, reaching ~90% of saturation in only 5 min. Similar kinetic profiles were previously observed for statherin (*40*). These very short-time adsorption measurements again suggest that the adsorption process is fast enough that the 4 min equilibration times used in ITC were sufficient for the process to reach equilibrium. One cannot rule out the possibility that the protein takes some time after adsorbing to convert to its lowest-energy structure so that the ultimate heat of adsorption may still be released more slowly. A second independent measurement of adsorption of statherin onto a HAP surface with a new batch of purified protein gave rise to similar binding isotherm curves. The measured binding enthalpy at 25 °C was higher at ca. 3.2 kcal/mol, and a slightly higher value for the α parameter (0.16−0.25 vs 0.11−0.21) was determined.

DISCUSSION

The ITC and the equilibrium adsorption isotherm results shown in this study indicate that only a fraction of the protein adsorbs to the mineral surface with detectable heat and that the majority of the protein adsorbs through a process that is thermo-neutral. The following discussion interprets this finding in the context of a two-binding site model that is implicitly based on the assumption of monolayer coverage limits. It has been previously observed that adsorption of statherin onto HAP gives ~130% coverage (*29*). This 30% difference or the 60% with N_{max} measured here falls within the monolayer range given the dispersion of the experimental adsorption data and the uncertainty of statherin dimensions and binding orientations. The structure of statherin is still unknown, and proteins may adsorb onto surfaces through a variety of orientations, i.e., side-on, end-on, partial attachment, etc. Molecular simulation programs which predict protein orientation on surfaces are just emerging (*41*, *42*). The binding isotherm reported here (Figure 3) is not characteristic of traditional multilayer adsorption isotherms, which are usually accompanied by a detectable step in concentration at monolayer completion (*15*, *27*).

To interpret the ITC and the equilibrium adsorption observations, we suggest that there are two types of adsorption sites for statherin on the mineral. One site, type A, comprises ~11−21% of the total adsorption sites on the mineral and is populated first with a constant exothermic heat of adsorption as measured by ITC. The other site, type B, displays a zero heat of adsorption and is populated primarily after the A sites are saturated. Given the intrinsic heterogeneity of the HAP surface, it is reasonable that there might be binding sites on HAP that are enthalpically more favorable and where protein molecules can preferably interact. These two different types of binding sites instead might be attributed to adsorption-induced surface heterogeneity. That is, at low coverage, the protein might adopt a conformation that is not permitted at higher coverage due to spatial (steric) limitations, although in this case the sites would not be completely independent as assumed above.

The thermodynamics of adsorption of statherin onto site A was determined from the heat detected upon titration (Figures 1 and 2 and Table 1). The adsorption is characterized by an exothermic heat of adsorption. However, this heat is relatively low, and it is therfore the entropy that makes the dominant contribution to the free energy of adsorption. Moreover, entropy is the only contribution to the adsorption process to site B. For all temperatures above 20 °C, the entropy contribution dominates adsorption even at the lowest fractional coverages where A sites dominate, and even below this temperature for all coverages above ~10% saturation.

Entropically driven adsorption onto HAP has been previously reported for two salivary proline rich phosphoproteins, PRP1 and PRP3 (*28*). The increase in entropy upon statherin adsorption may arise from displacement of water molecules from the HAP surface and the protein molecule to the bulk solution. The contribution to the entropy from changes in the immobilization of the protein itself is expected to have the opposite effect, due to the loss of orientational and translational entropy of the protein upon adsorption. However, partial denaturation of the protein upon adsorption could give rise to increased configurational entropy. While solid-state NMR measurements of statherin adsorbed onto hydroxyapatite demonstrated that the N-terminal domain of the protein is α-helical (*13*), CD spectroscopy analysis of statherin in aqueous solution (no HAP) indicated an essentially disordered peptide structure (*8*, *9*). It is therefore reasonable that conformational changes in the protein during adsorption might also contribute to the entropy change. Ongoing high-resolution structure analysis of free and bound statherin will clarify the extent of these changes.

The change in entropy due to the loss of the water of hydration, ΔS_{hyd}, can be estimated by multiplying the number of water molecules released to the bulk upon adsorption by $-(S_h - S_0)$, the average difference in the partial molar entropy between the water of protein hydration and bulk water. The data on entropy of hydration of different amino acid groups presented by Makhatadze and Privalov (*43*) suggest that at 25 °C, the value of $-(S_h - S_0)$ is essentially independent of the chemical nature of a solvent-exposed atomic group and on average equals 1.3 ± 0.3 cal K^{-1} mol^{-1}. We estimate the number of water molecules released upon statherin adsorption by assuming a loss of solvent-accessible surface area equal to its cross-sectional area on the mineral, assuming it is globular (2.64 nm^2, calculated based on the observed N_{max}) and assuming that there are 2.5 water molecules of hydration for every 0.09 nm^2 of solvent-accessible area, based on the work of Filfil and Chalikian (*44*). This gives 73 water molecules released per statherin molecule and a corresponding entropy contribution of 95 cal K^{-1} mol^{-1} in statherin adsorption. This can be compared to the observed entropy increase of ~23 cal K^{-1} mol^{-1} from Table 1 at 25 °C. The 4-fold difference might be explained as being due to the fact that not all the water of hydration in the area of the statherin−HAP contact is lost as bulk water upon adsorption; instead, only ~25% are lost.

We have shown that the apparent heat change of adsorption to site A depends on the buffer in which the experiment is carried out (Figure 7 and Table 4) and therfore concluded that the adsorption process involves proton transfer, a

common phenomenon in adsorption of proteins onto surfaces (*27*). From the known ionization heat of the buffers used, we could determine that approximately one proton is being taken up by the interacting species per protein molecule in the course of adsorption. At this point, we cannot tell if a proton is taken up by the mineral or by the protein and which amino acids are involved in that process. Future ITC studies on statherin mutants are aimed at unraveling that. The involvment of proton transfer in the adsorption process of statherin may play a significant biological role as the saliva environment is subjected to significant pH variations.

The temperature dependence of the adsorption thermodynamics determined from ITC shows that the enthalpy change upon adsorption to site A becomes less exothermic with an increase in temperature (Figures 2 and 6 and Table 1). The change in enthalpy with temperature resulted in a ΔC_p value of 194 ± 7 cal K^{-1} mol^{-1} at 25 °C (Table 3). This positive ΔC_p together with the observed positive ΔS is inconsistent with this interaction being dominated by hydrophobic interactions common to protein−protein and protein−ligand interactions (*45*, *46*). However, from the study of protein interactions dominated by electrostatics, it is known that a positive heat capacity change and a positive ΔS accompany burial of polar groups (*45*, *47*−*50)*. A positive ΔC_p value of 286 ± 27 cal K^{-1} mol^{-1} has been previously observed for adsorption of cytochrome b_5 onto an anion exchange surface at low coverage (*18*). It is reasonable that the positive ΔC_p value observed here reflects a similar electrostatic interaction between the negatively charged N-terminus of statherin and the ionic hydroxyapatite surface sites. If water that is hydrating polar groups is lost upon adsorption (due to burial of polar groups on the surfaces of the protein and HAP upon association), then one expects to see an increase in C_p because the hydration of polar groups has a negative ΔC_p (*47*, *48*). Such a process is also known to be characterized by a positive entropy, as observed here (*48*, *50*).

It is interesting that there is an increase in the equilibrium constant that accompanies increasing coverage of the B sites. The β values in Table 2 show that the equilibrium constant increases 3−17-fold with coverage, corresponding to an increase in the magnitude of $\Delta G°$ of ∼0.40−0.85 kcal/mol. This could be associated with attractive forces between coadsorbed protein molecules. The dimerization of statherin has been previously reported in solution (*51*), and such attractive forces could also occur in the adsorbed layer. Those attractive interactions might particularly be associated with the high prevalence of hydrophobic residues in the middle and C-terminal parts of the protein (*1*, *5*). We propose that at higher coverage, hydrophobic interactions are formed between coadsorbed protein molecules upon adsorption. Also consistent with the data is the fact that such interactions are usually characterized by a high entropy due to the release of bound water to the solution (*48*, *50*). The enthalpy of such interactions is composed of the enthalpy of packing of hydrophobic residues and the dehydration enthalpies of different residues. These two enthalpies are expected to have opposite signs (*52*) which could explain the approximately zero enthalpy observed for the B site binding regime.

CONCLUSION

We have demonstrated that isothermal titration calorimetry can be used as a sensitive probe to study the thermodynamics of adsorption of statherin onto its natural mineral substrate hydroxyapatite. Moreover, combining the results obtained from binding isotherm analysis and ITC gave insight into the underlying processes involved in the adsorption process. We suggest that at low coverage statherin adsorbs onto HAP with a significant favorable free energy change that is driven by both entropy and enthalpy. With increased coverage, the adsorption remains spontaneous but is driven entropically, which we attribute to the loss of bound water molecules. The high affinity of the protein to the mineral at low coverage may explain previous observations where low coverages of statherin were sufficient to control HAP crystal growth (*4*, *5*). Moreover, the relatively low magnitude of the enthalpy for binding at low coverage might play a role in the dynamics of the adsorption processes, where reversibility allows functional responses to saliva conditions that are strongly time and condition dependent. The involvement of proton transfer in the adsorption process is biologically significant as well given the fact that the saliva is exposed to major variations in pH. These studies provide a strong basis for future statherin structure−function studies.

ACKNOWLEDGMENT

We thank Prof. Joseph A. Beavo and Dr. Thomas R. Hinds for kindly permitting the use of their isothermal titration microcalorimeter. We acknowledge Dr. Allison Campbell from the Battelle Pacific Northwest National Laboratory for providing us with the hydroxyapatite samples and Dr. Wendy Shaw for fruitful discussions. We thank Dr. Verna Frasca and Dr. Lung-Nan Lin from Microcal, LLC, for the DSC measurements and analysis. We also thank Mr. Robert Britschgi for help with protein synthesis and purification and Dr. Martin Sadilek for help with mass spectrometry analysis of the protein.

REFERENCES

1. Schlesinger, D. H., and Hay, D. I. (1977) Complete covalent structure of statherin, a tyrosine-rich acidic peptide which inhibits calcium phosphate precipitation from human parotid saliva, *J. Biol. Chem. 252*, 1689−1695.
2. Hay, D. I., Smith, D. J., Schluckebier, S. K., and Moreno, E. C. (1984) Relationship between concentration of human salivary statherin and inhibition of calcium phosphate precipitation in stimulated human parotid saliva, *J. Dent. Res. 63*, 857−863.
3. Schlesinger, D. H., Hay, D. I., and Levine, M. J. (1989) Complete primary structure of statherin, a potent inhibitor of calcium phosphate precipitation, from the saliva of the monkey, *Macaca arctoides*, *Int. J. Pept. Protein Res. 34*, 374−380.
4. Johnsson, M., Richardson, C. F., Bergey, E. J., Levine, M. J., and Nancollas, G. H. (1991) The effects of human salivary cystatins and statherin on hydroxyapatite crystallization, *Arch. Oral Biol. 36*, 631−636.
5. Raj, P. A., Johnsson, M., Levine, M. J., and Nancollas, G. H. (1992) Salivary statherin. Dependence on sequence, charge, hydrogen bonding potency, and helical conformation for adsorption to hydroxyapatite and inhibition of mineralization, *J. Biol. Chem. 267*, 5968−5976.
6. Schwartz, S. S., Hay, D. I., and Schluckebier, S. K. (1992) Inhibition of calcium phosphate precipitation by human salivary statherin: Structure−activity relationships, *Calcif. Tissue Int. 50*, 511−517.
7. Wikiel, K., Burke, E. M., Perich, J. W., Reynolds, E. C., and Nancollas, G. H. (1994) Hydroxyapatite mineralization and demineralization in the presence of synthetic phosphorylated pentapeptides, *Arch. Oral Biol. 39*, 715−721.
8. Gururaja, T. L., and Levine, M. J. (1996) Solid-phase synthesis and characterization of human salivary statherin: A tyrosine-rich

phosphoprotein inhibitor of calcium phosphate precipitation, *Pept. Res. 9*, 283−289.
9. Naganagowda, G. A., Gururaga, T. L., and Levine, M. J. (1998) Delineation of conformational preferences in human salivary statherin by ^{1}H, ^{31}P NMR and CD studies: Sequential assignment and structure−function correlations, *J. Biomol. Struct. Dyn. 16*, 91−107.
10. Long, J. R., Dindot, J. L., Zebroski, H., Kiihne, S., Clark, R. H., Campbell, A. A., Stayton, P. S., and Drobny, G. P. (1998) A peptide that inhibits hydroxyapatite growth is in an extended conformation on the crystal surface, *Proc. Natl. Acad. Sci. U.S.A. 95*, 12083−12087.
11. Shaw, W. J., Long, J. R., Dindot, J. L., Campbell, A. A., Stayton, P. S., and Drobny, G. P. (2000) Determination of Statherin N-Terminal Peptide Conformation on Hydroxyapatite Crystals, *J. Am. Chem. Soc. 122*, 1709−1716.
12. Shaw, W. J., Long, J. R., Campbell, A. A., Stayton, P. S., and Drobny, G. P. (2000) A Solid State NMR Study of Dynamics in a Hydrated Salivary Peptide Adsorbed to Hydroxyapatite, *J. Am. Chem. Soc. 122*, 7118−7119.
13. Long, J. R., Shaw, W. J., Stayton, P. S., and Drobny, G. P. (2001) Structure and dynamics of hydrated statherin on hydroxyapatite as determined by solid-state NMR, *Biochemistry 40*, 15451−15455.
14. Gibson, J. M., Raghunathan, V., Popham, J. M., Stayton, P. S., and Drobny, G. P. (2005) A REDOR NMR study of a phosphorylated statherin fragment bound to hydroxyapatite crystals, *J. Am. Chem. Soc. 127*, 9350−9351.
15. Norde, W. (1986) Adsorption of proteins from solution at the solid−liquid interface, *Adv. Colloid Interface Sci. 25*, 267−340.
16. Lin, F. Y., Chen, W. Y., and Hearn, M. T. (2002) Thermodynamic analysis of the interaction between proteins and solid surfaces: Application to liquid chromatography, *J. Mol. Recognit. 15*, 55−93.
17. Lin, F. Y., Chen, W. Y., and Hearn, M. T. W. (2001) Microcalorimetric Studies on the Interaction Mechanism between Proteins and Hydrophobic Solid Surfaces in Hydrophobic Interaction Chromatography: Effects of Salts, Hydrophobicity of the Sorbent, and Structure of the Protein, *Anal. Chem. 73*, 3875−3883.
18. Gill, D. S., Roush, D. J., Shick, K. A., and Willson, R. C. (1995) Microcalorimetric characterization of the anion-exchange adsorption of recombinant cytochrome b_5 and its surface-charge mutants, *J. Chromatogr., A 715*, 81−93.
19. Bowen, W. R., and Hughes, D. T. (1993) Ion exchange of proteins: A microcalorimetric study of the adsorption of bovine serum albumin on anion-exchange materials, *J. Colloid Interface Sci. 158*, 395−402.
20. Lee, V. A., Craig, R. G., Filisko, F. E., and Zand, R. (2005) Microcalorimetry of the adsorption of lysozyme onto polymeric substrates, *J. Colloid Interface Sci. 288*, 6−13.
21. Norde, W., and Lyklema, J. (1978) The adsorption of human plasma albumin and bovine pancreas ribonuclease at negatively charged polystyrene surfaces: I. Adsorption isotherms. effects of charge, ionic strength, and temperature, *J. Colloid Interface Sci. 66*, 257−265.
22. Norde, W., and Lyklema, J. (1978) The adsorption of human plasma albumin and bovine pancreas ribonuclease at negatively charged polystyrene surfaces: IV. The charge distribution in the adsorbed state, *J. Colloid Interface Sci. 66*, 285−294.
23. Norde, W., and Lyklema, J. (1978) The adsorption of human plasma albumin and bovine pancreas ribonuclease at negatively charged polystyrene surfaces: V. Microcalorimetry, *J. Colloid Interface Sci. 66*, 295−302.
24. Koutsoukos, P. G., Norde, W., and Lyklema, J. (1983) Protein adsorption on hematite (α-Fe_2O_3) surfaces, *J. Colloid Interface Sci. 95*, 385−397.
25. Nyilas, E., Chiu, T. H., and Herzlinger, G. A. (1974) Thermodynamics of native protein/foreign surface interactions. I. Calorimetry of the human γ-globulin/glass system, *Trans.−Am. Soc. Artif. Intern. Organs 20B*, 480−490.
26. Chiu, T. H., Nyilas, E., and Lederman, D. M. (1976) Thermodynamics of native protein/foreign surface interactions. IV. Calorimetric and microelectrophoretic study of human fibrinogen sorption onto glass and LTI-carbon, *Trans.−Am. Soc. Artif. Intern. Organs 22*, 498−513.
27. Haynes, C. A., and Norde, W. (1995) Structures and Stabilities of Adsorbed Proteins, *J. Colloid Interface Sci. 169*, 313−328.
28. Moreno, E. C., Kresak, M., and Hay, D. I. (1984) Adsorption of molecules of biological interest onto hydroxyapatite, *Calcif. Tissue Int. 36*, 48−59.
29. Moreno, E. C., Kresak, M., and Hay, D. I. (1978) Adsorption of two human parotid salivary macromolecules on hydroxy-, fluorhydroxy- and fluorapatites, *Arch. Oral Biol. 23*, 525−533.
30. Johnsson, M., Levine, M. J., and Nancollas, G. H. (1993) Hydroxyapatite binding domains in salivary proteins, *Crit. Rev. Oral Biol. Med. 4*, 371−378.
31. Ebrahimpour, A., Johnsson, M., Richardson, C. F., and Nancollas, G. H. (1993) The characterization of hydroxyapatite preparations, *J. Colloid Interface Sci. 159*, 158−163.
32. Wiseman, T., Williston, S., Brandts, J. F., and Lin, L. N. (1989) Rapid measurement of binding constants and heats of binding using a new titration calorimeter, *Anal. Biochem. 179*, 131−137.
33. Olsson, D. M., and Nelson, L. S. (1975) Nelder-Mead simplex procedure for function minimization, *Technometrics 17*, 45−51.
34. Gray, J. J. (2004) The interaction of proteins with solid surfaces, *Curr. Opin. Struct. Biol. 14*, 110−115.
35. Mura-Galelli, M. J., Voegel, J. C., Behr, S., Bres, E. F., and Schaaf, P. (1991) Adsorption/desorption of human serum albumin on hydroxyapatite: A critical analysis of the Langmuir model, *Proc. Natl. Acad. Sci. U.S.A. 88*, 5557−5561.
36. Ramsden, J. J. (1995) Puzzles and paradoxes in protein adsorption, *Chem. Soc. Rev. 24*, 73−78.
37. Pierce, M. M., Raman, C. S., and Nall, B. T. (1999) Isothermal Titration Calorimetry of Protein−Protein Interactions, *Methods 19*, 213−221.
38. Sturtevant, J. M., and Beres, L. (1971) Calorimetric studies of the activation of chymotrypsinogen A, *Biochemistry 10*, 2120−2126.
39. Fukada, H., and Takahashi, K. (1998) Enthalpy and heat capacity changes for the proton dissociation of various buffer components in 0.1 M potassium chloride, *Proteins 33*, 159−166.
40. Lamkin, M. S., Arancillo, A. A., and Oppenheim, F. G. (1996) Temporal and compositional characteristics of salivary protein adsorption to hydroxyapatite, *J. Dent. Res. 75*, 803−808.
41. Minton, A. P. (1999) Adsorption of Globular Proteins on Locally Planar Surfaces. II. Models for the Effect of Multiple Adsorbate Conformations on Adsorption Equilibria and Kinetics, *Biophys. J. 76*, 176−187.
42. Sun, Y., Welsh, W. J., and Latour, R. A. (2005) Prediction of the Orientations of Adsorbed Protein Using an Empirical Energy Function with Implicit Solvation, *Langmuir 21*, 5616−5626.
43. Makhatadze, G. I., and Privalov, P. L. (1995) Energetics of protein structure, *Adv. Protein Chem. 47*, 307−425.
44. Filfil, R., and Chalikian, T. V. (2003) The Thermodynamics of Protein−Protein Recognition as Characterized by a Combination of Volumetric and Calorimetric Techniques: The Binding of Turkey Ovomucoid Third Domain to α-Chymotrypsin, *J. Mol. Biol. 326*, 1271−1288.
45. Loladze, V. V., Ermolenko, D. N., and Makhatadze, G. I. (2001) Heat capacity changes upon burial of polar and nonpolar groups in proteins, *Protein Sci. 10*, 1343−1352.
46. Sturtevant, J. M. (1977) Heat capacity and entropy changes in processes involving proteins, *Proc. Natl. Acad. Sci. U.S.A. 74*, 2236−2240.
47. Sharp, K. A., and Madan, B. (1997) Hydrophobic Effect, Water Structure, and Heat Capacity Changes, *J. Phys. Chem. B 101*, 4343−4348.
48. Robinson, G. W., and Cho, C. H. (1999) Role of Hydration Water in Protein Unfolding, *Biophys. J. 77*, 3311−3318.
49. Prabhu, N. V., and Sharp, K. I. (2005) Heat capacity in proteins, *Annu. Rev. Phys. Chem. 56*, 521−548.
50. Makhatadze, G. M., and Privalov, P. L. (1993) Contribution of Hydration to Protein Folding Thermodynamics II. The Entropy and Gibbs Energy of Hydration, *J. Mol. Biol. 232*, 660−679.
51. Hay, D. I. (1973) The isolation from human parotid saliva of a tyrosine-rich acidic peptide which exhibits high affinity for hydroxyapatite surfaces**,** *Arch. Oral Biol. 18*, 1531−1540.
52. Makhatadze, G. M., and Privalov, P. L. (1993) Contribution of Hydration to Protein Folding Thermodynamics I. The Enthalpy of Hydration, *J. Mol. Biol. 232*, 639−659.

BI052321Z